Letter

Structural analysis of conformational changes in the mpox virus A7 protein

Xincheng Ni, Kai Wang, Yinze Han, Jian Lei [*]

National Clinical Research Center for Geriatrics, and State Key Laboratory of Biotherapy and Cancer Center, West China Hospital, Sichuan University, Chengdu, 610041, China

Dear Editor,

The mpox (formerly known as monkeypox) disease caused by the mpox virus (MPXV) has infected more than 89,700 people and is linked to 157 deaths in 114 countries worldwide as of September 2023 (www.who.int). Mpox is a zoonotic disease, the first human case of which was reported in 1970 (Breman et al., 1980). Common symptoms in mpox-infected individuals include fever, myalgia, fatigue, headache, and a characteristic rash (Isidro et al., 2022). Current treatments for mpox remain limited, and an in-depth investigation of essential viral protein(s) will help to explore novel drug targets.

MPXV is an enveloped double-stranded DNA virus, belonging to the genus *Orthopoxvirus* and family *Poxviridae* (Isidro et al., 2022). It has a genome approximately 200 kb in size and encodes around 200 proteins (Kugelman et al., 2014). Poxviruses acquire their primary envelopes by extending crescent membranes (Condit et al., 2006; Moss, 2015), the stable open-ended membranes derived from endoplasmic reticulum (ER) rupture (Krijnse Locker et al., 2013; Weisberg et al., 2017). Crescent membranes play key roles in the formation of spherical immature virions (IVs) that condense into mature virions (MVs) (Meng et al., 2007). A group of conserved proteins, including A6, A11, A30.5, H7, and L2, is essential for formation of crescent membranes in vaccinia viruses (VACV, the prototype virus in *Poxviridae*) (Wu et al., 2012; Maruri-Avidal et al., 2013; Kolli et al., 2015; Meng et al., 2017; Pathak et al., 2018). Collectively, these proteins are known as viral membrane assembly proteins (VMAPs) (Maruri-Avidal et al., 2013; Moss, 2015).

A6, as the largest VMAP component, functions in both crescent membrane formation and the enclosure process to form immature virions. A6 localizes predominantly in the cytosol (Meng et al., 2007, 2012) and consists of two separate domains: an N-terminal domain (A6N) and a C-terminal domain (A6C) (Meng et al., 2017). The A6N is indispensable for intact viral membrane assembly. The absence of A6N in VACV or its replacement with the homologous region from Yaba-like disease virus (YLDV) leads to a failure of viral replication (Meng et al., 2017). Meanwhile, the A6C presents a cage-like conformation that captures phospholipids, including phosphatidylethanolamine (PE) and phosphatidylglycerol (PG), in a bilayer-like configuration (Pathak et al.,

2018). Moreover, A6 interacts with another VMAP component, A11, thus regulating the membrane association of the latter protein in VACV (Wu et al., 2012).

Currently, structural information on the poxvirus A6 protein is limited. To the best of our knowledge, only crystal structures of the N-terminal domain of VACV A6 and the C-terminal domain of FPV170 (A6 ortholog of fowlpox virus) have been reported (Pathak et al., 2018). In this study, to expand structural and functional information on the A6 homolog of MPXV (designated as A7 protein), we first constructed two separate A7 truncations (Fig. 1A), A7N$_{121}$ (residues 1–121, corresponding to A6N of VACV) and A7C (residues 122–372, corresponding to A6C of VACV), according to previous research (Meng et al., 2017). We purified MPXV A7 as well as its two truncations *in vitro*, analyzing these proteins via size-exclusion chromatography (SEC) (Fig. 1B). The SEC results indicated that A7 (~43.4 kDa), A7N$_{121}$ (~14.3 kDa), and A7C (~29.4 kDa) were monomeric in solution with reference to the standard proteins of 44.0 kDa, 29.0 kDa and 13.7 kDa (Fig. 1B). The quality of these proteins was assessed using SDS-PAGE.

Previous studies have shown that VACV A6 and FPV170 possess phospholipid-binding ability, and that the A6C and its ortholog region are responsible for lipid binding (Pathak et al., 2018). To determine whether MPXV A7 has phospholipid-binding ability and identify the lipid-binding region, freshly purified A7, A7N$_{121}$, and A7C were incubated with fluorescently labeled PE, respectively. The lipid-binding levels of these proteins were visualized using native-PAGE (Fig. 1C). Groups, where the full-length A7 or the truncated A7C was added, showed distinct phospholipid bands compared to the control group with PE alone, whereas the group with A7N$_{121}$ presented no phospholipid binding (Fig. 1C). These findings demonstrate that, similarly to homologous proteins in other poxviruses, the MPXV A7 protein has phospholipid-binding ability, and the C-terminal domain is the only lipid-interacting region.

To illustrate the structural information on MPXV A7, we crystallized the full-length A7, A7N$_{121}$, and A7C, respectively. Finally, we obtained the crystals of A7N$_{121}$ and A7C, solving the structure of A7N$_{121}$ at approximately 1.7 Å (Fig. 1D). However, the crystals of A7C displayed no

---
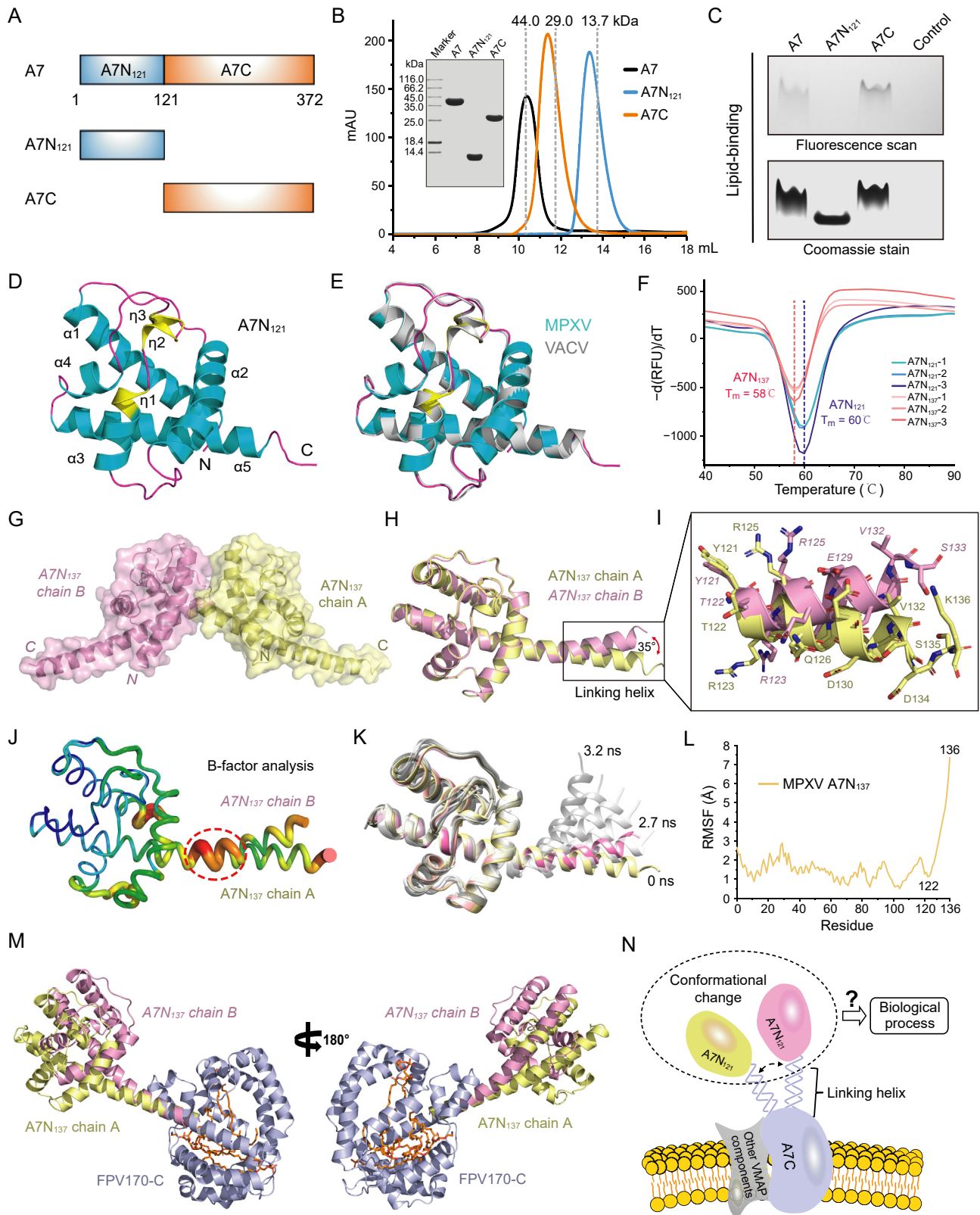
(caption on next page)

Fig. 1. Structural analysis of conformational changes in MPXV A7 protein. **A** Schematic representation of MPXV A7 domains. The N-terminal domain (A7N$_{121}$) and C-terminal domain (A7C) are illustrated. **B** The oligomeric status of A7 and its truncations in solution were analyzed via SEC assays. Full-length A7: ~43.4 kDa. A7N$_{121}$: ~14.3 kDa. A7C: ~29.4 kDa. The peak positions of three standard proteins are shown as gray dashed lines. The quality of these proteins was assessed using SDS-PAGE. **C** Lipid-binding analysis of MPXV A7, A7N$_{121}$ and A7C. Top panel, fluorescence scan. Bottom panel, coomassie stain of the same gel. **D** Crystal structure of the MPXV A7N$_{121}$. The secondary structures are labeled. The α-helices, 3$_{10}$ helices, and loops are indicated in cyan, yellow, and magenta, respectively. **E** Structural comparison between MPXV A7N$_{121}$ and its homologous protein in VACV (PDB code: 6CB6). **F** Differential scanning fluorimetry analysis of A7N$_{121}$ and A7N$_{137}$. Melting peaks of A7N$_{121}$ and A7N$_{137}$ from three independent experiments ($n = 3$) are indicated, and T$_m$ values of A7N$_{121}$ and A7N$_{137}$ are highlighted with blue and red dashed lines, respectively. **G** Overall structures of two A7N$_{137}$ molecules in the asymmetric unit. The two A7N$_{137}$ are displayed in yellow (chain A) and pink (chain B). The N- and C-termini of both chains are marked in the corresponding colors. **H** Superimposing two A7N$_{137}$ chains revealed a conformational wobble in the C-terminal helix region. **I** Zoom-in view of the conformational changes in the linking helix. Residues Tyr121–Lys136 in chain A and Tyr121–Ser133 in chain B are shown in sticks. **J** The B-factor analysis of two A7N$_{137}$ chains. The flexible hinge (residues Leu117 to Thr122) is indicated by a red dashed circle. **K** Overlay of the A7N$_{137}$ snapshots at different molecular dynamics (MD) simulation moments. The simulated conformations of A7N$_{137}$ are shown in gray with gradient transparency, and the chain-A and chain-B A7N$_{137}$ are colored in yellow and pink, respectively. **L** Root mean square fluctuations (RMSF) of A7N$_{137}$ each residue in MD simulation. **M** Superimposing each of two MPXV A7N$_{137}$ structures (PDB code: 8IZU) onto the phospholipid-bound FPV170-C structure (PDB code: 6BR8, chain A) enables the illustration of a hypothetical model of full-length A7. The chain-A A7N$_{137}$, chain-B A7N$_{137}$, FPV170-C, and phospholipids are colored in yellow, pink, purple, and orange, respectively. **N** A proposed model of A7 protein interacting with the phospholipid bilayer. The conformational wobble of A7N$_{121}$ is indicated by a double dashed arrow. Figures (**D**, **E**, **G-J**, and **M**) were prepared using PyMOL (https://pymol.org). Figure **K** was prepared using Chimera (http://www.cgl.ucsf.edu/chimera/). Experimental details were provided in the Supplementary materials.

---

diffraction points, probably due to conformational heterogeneity caused by the binding of endogenous phospholipids derived from *Escherichia coli*. The diffraction parameters and refinement statistics of A7N$_{121}$ are summarized in Table 1. Only one molecule exists in the asymmetric unit (ASU) of the A7N$_{121}$ crystal. In the final refined model, residues 1–121 were successfully built. The overall shape of A7N$_{121}$ presents a compact conformation and resembles the letter "a" (Fig. 1D). According to the DSSP server (https://swift.cmbi.umcn.nl/gv/dssp), A7N$_{121}$ consists of five α-helices and three 3$_{10}$ helices in the order: α1–α2–α3–η1–η2–α3–α4–α5 (η: 3$_{10}$ helix). Of these, helices α1, α2 and α5 are obviously longer than other helices. The side chains of residues Glu58 and Cys69 showed double conformations. The overall structure of MPXV A7N$_{121}$ was very similar to that of VACV A6N (Fig. 1E), with the root mean square deviation (RMSD) value is about 0.4 Å according to all Cαs.

Based on analysis of the MPXV A7N$_{121}$ structure, we found that the C-terminal part of A7N$_{121}$ was present as an α-helix (albeit several residues unwound to a disordered coil, Fig. 1D). In VACV A6N, Pathak et al. found that the C-terminal region presented as an α-helix in the C2 but a loop in

the P4$_1$2$_1$2 space group, suggesting a dynamic connection may exist between A6N and A6C (Pathak et al., 2018). In parallel, we noticed that the N-terminus of FPV170-C contained an α-helix. Thus, we speculated that it is likely that the two domains of MPXV A7 are connected by a long helix. Accordingly, it is necessary to investigate the mode of attachment of A7N$_{121}$ and A7C as well as the relative orientations between these two domains.

To explore the connection region between MPXV A7N$_{121}$ and A7C, we constructed and purified a new A7 truncation, A7N$_{137}$ (residues 1–137), which contained the linking region connected to A7N$_{121}$ and A7C. We analyzed the protein stabilities of A7N$_{121}$ and A7N$_{137}$ using the differential scanning fluorimetry assays (Fig. 1F). We found that the melting temperature of A7N$_{137}$ (T$_m$ = 58 °C) was decreased by 2 °C compared with that of A7N$_{121}$ (T$_m$ = 60 °C), suggesting that the presence of the linking region (^{122}TRLRQDTEDIVSDSKK^{137}) may reduce the overall protein stability. We further determined the crystal structure of A7N$_{137}$ at ~2.5 Å resolution to describe the structural information of the linking region (Fig. 1G). Two A7N$_{137}$ molecules were presented in the ASU of the crystal, named chain A and chain B, respectively. Residues 1–136 in chain A and 1–133 in chain B were successfully built into our final models, and the overall structures of the two A7N$_{137}$ chains were almost identical, with RMSD value of approximately 0.3 Å according to all Cαs. Intriguingly, although the linking regions of both protomers were presented as α-helices, the helices showed a significant conformational wobble with a varied angle of approximately 35° (calculated from the included angle between the Cα atoms of Asp134 (chain A), Val132 (chain B), and Tyr121 (the overlapping Cα atoms of chains A and B)) (Fig. 1H). The residues of these two linking helices in both A7N$_{137}$ chains are shown as sticks to better observe the conformational changes (Fig. 1I), and the *2Fo – Fc* electron density maps corresponding to these parts are displayed in Supplementary Figure S1.

Subsequently, we investigated the B-factor parameters of both A7N$_{137}$ chains and found that residues Leu117 to Thr122 possess much higher B-factor values (Fig. 1J), indicating the intrinsic flexibility of this region (Fig. 1J). The linking helix of A7N$_{137}$ possesses few interactions with other parts of protein, suggesting the possibility of its conformational changes. Furthermore, we performed a molecular dynamics (MD) simulation to predict the potential movements of A7N$_{137}$ (Fig. 1K). The chain A (in yellow) of A7N$_{137}$ was used as the initial conformation, we found that the linking helix of A7N$_{137}$ underwent a significant up-and-down swing within the first 10 nanosecond (ns) and later reached the stable status (Supplementary Movie S1). Notably, the conformation at 2.7 ns during the simulation was perfectly consistent with the conformation of chain-B A7N$_{137}$ (in pink, Fig. 1K). We used root mean square fluctuation (RMSF) to quantify the positional differences of each residue in the MD simulation (Fig. 1L), and found that the RMSF values were increased dramatically from Thr122 to Lys136, which is consistent with the

Table 1
Data collection and refinement statistics.

	A7N$_{121}$	A7N$_{137}$
Data collection		
Space group	*C 2*	*C 2 2 2$_1$*
Cell dimensions		
a, b, c (Å)	76.0, 31.3, 49.8	37.9, 140.3, 153.5
α, β, γ (°)	*β* = 112.3	
Resolution (Å)	46.10-1.74 (1.77-1.74)	19.45-2.54 (2.65-2.54)
R$_{merge}$	0.069 (0.770)	0.108 (0.785)
Mean *I*/σ(*I*)	15.0 (2.4)	14.1 (3.5)
Unique reflections	10,782 (612)	14,013 (1676)
Completeness (%)	95.2 (99.7)	99.8 (99.9)
Redundancy	6.2 (5.4)	12.8 (12.9)
Refinement		
Resolution (Å)	35.10-1.74	19.45-2.54
R$_{factor}$/R$_{free}$	0.180/0.205	0.210/0.239
No. atoms		
Protein	1002	2229
Water	146	87
Average *B*-factor (Å^2)	23.0	74.0
R.m.s. deviations		
Bond lengths (Å)	0.010	0.010
Bond angles (°)	1.539	1.578
Ramachandran favored (%)	98.4	98.5
Ramachandran allowed (%)	1.6	1.5
Ramachandran outliers (%)	0.0	0.0
PDB code	8IZT	8IZU

Values in parentheses are for highest resolution shell.

$R_{factor} = \sum_{hkl} |F_o(hkl) - F_c(hkl)| / \sum_{hkl} |F_o(hkl)|$.

R_{free} was calculated for a test set of reflections (~5.0%) omitted from the refinement.

conformation wobble helix in our crystal structures (Fig. 1I). Meanwhile, the residues of the linking helix are conserved in poxviruses from different genera (Supplementary Figure S2), particularly in the genus *Orthopoxvirus* [including MPXV, VACV and variola virus (VARV)], suggesting that dynamic characteristics of this linking helix could exist in various poxviruses.

To illustrate the influence of wobble linking-helix conformations on the A7 protein, we proposed a full-length A7 model by superimposing each of the two MPXV $A7N_{137}$ structures onto the phospholipid-bound FPV170-C structure, and described the relative positions of $A7N_{121}$ and A7C (Fig. 1M). According to this model, conformational changes in the linking helix could result in an obvious movement of $A7N_{121}$ relative to the bilayer phospholipid-bound A7C, which may help $A7N_{121}$ perform its function(s) (Fig. 1N), such as engagement in virion morphogenesis, binding to viral partners, or transmitting signals. Previous studies reported that the conformational shifts of α-helix do play a critical role in biological functions. For example, the conformational changes of the α7 helix in integrin could alter the relative orientations between its β1 and hybrid domains, involving in biological signals transmission (Luo and Springer, 2006). Thus, it is worth investigating the exact function(s) derived from the various relative positions of two subdomains in A7.

Along with the COVID-19 outbreak, the ongoing mpox pandemic continues to threaten human health. MPXV A7 is the largest viral membrane assembly protein and plays key roles in virion morphogenesis. In this study, we investigated the phospholipid-binding ability of MPXV A7 protein. We determined the crystal structures of two N-terminal truncates of A7, $A7N_{121}$ and $A7N_{137}$. Based on the latter structure, we found that the conserved region of residues 122–137 in $A7N_{137}$ displayed obvious conformational changes, leading to different relative orientations between the N- and C-terminal domains of A7. We further performed the MD stimulation to analyze potential movements of the residues 122–137 region. Finally, we proposed a structural model of the full-length A7 protein and discussed its potential biological roles derived from the various intrinsic relative orientations between its two domains. In conclusion, our study expands the current knowledge on MPXV A7 protein, and provides a foundation for further investigations into the detailed biological functions of A7.

Footnotes

References

Breman, J.G., Kalisa-Ruti, Steniowski, M.V., Zanotto, E., Gromyko, A.I., Arita, I., 1980. Human monkeypox, 1970-79. Bull. World Health Organ. 58, 165–182.

Condit, R.C., Moussatche, N., Traktman, P., 2006. In a nutshell: structure and assembly of the vaccinia virion. Adv. Virus Res. 66, 31–124.

Isidro, J., Borges, V., Pinto, M., Sobral, D., Santos, J.D., Nunes, A., Mixão, V., Ferreira, R., Santos, D., Duarte, S., Vieira, L., Borrego, M.J., Núncio, S., de Carvalho, I.L., Pelerito, A., Cordeiro, R., Gomes, J.P., 2022. Phylogenomic characterization and signs of microevolution in the 2022 multi-country outbreak of monkeypox virus. Nat. Med. 28, 1569–1572.

Kolli, S., Meng, X., Wu, X., Shengjuler, D., Cameron, C.E., Xiang, Y., Deng, J., 2015. Structure-function analysis of vaccinia virus H7 protein reveals a novel phosphoinositide binding fold essential for poxvirus replication. J. Virol. 89, 2209–2219.

Krijnse Locker, J., Chlanda, P., Sachsenheimer, T., Brügger, B., 2013. Poxvirus membrane biogenesis: rupture not disruption. Cell Microbiol. 15, 190–199.

Kugelman, J.R., Johnston, S.C., Mulembakani, P.M., Kisalu, N., Lee, M.S., Koroleva, G., McCarthy, S.E., Gestole, M.C., Wolfe, N.D., Fair, J.N., Schneider, B.S., Wright, L.L., Huggins, J., Whitehouse, C.A., Wemakoy, E.O., Muyembe-Tamfum, J.J., Hensley, L.E., Palacios, G.F., Rimoin, A.W., 2014. Genomic variability of monkeypox virus among humans, Democratic Republic of the Congo. Emerg. Infect. Dis. 20, 232–239.

Luo, B.H., Springer, T.A., 2006. Integrin structures and conformational signaling. Curr. Opin. Cell Biol. 18, 579–586.

Maruri-Avidal, L., Weisberg, A.S., Moss, B., 2013. Association of the vaccinia virus A11 protein with the endoplasmic reticulum and crescent precursors of immature virions. J. Virol. 87, 10195–10206.

Meng, X., Embry, A., Sochia, D., Xiang, Y., 2007. Vaccinia virus A6L encodes a virion core protein required for formation of mature virion. J. Virol. 81, 1433–1443.

Meng, X., Embry, A., Rose, L., Yan, B., Xu, C., Xiang, Y., 2012. Vaccinia virus A6 is essential for virion membrane biogenesis and localization of virion membrane proteins to sites of virion assembly. J. Virol. 86, 5603–5613.

Meng, X., Rose, L., Han, Y., Deng, J., Xiang, Y., 2017. Vaccinia virus A6 is a two-domain protein requiring a cognate N-terminal domain for full viral membrane assembly activity. J. Virol. 91, e02405–e02416.

Moss, B., 2015. Poxvirus membrane biogenesis. Virology 479–480, 619–626.

Pathak, P.K., Peng, S., Meng, X., Han, Y., Zhang, B., Zhang, F., Xiang, Y., Deng, J., 2018. Structure of a lipid-bound viral membrane assembly protein reveals a modality for enclosing the lipid bilayer. Proc. Natl. Acad. Sci. U.S.A. 115, 7028–7032.

Weisberg, A.S., Maruri-Avidal, L., Bisht, H., Hansen, B.T., Schwartz, C.L., Fischer, E.R., Meng, X., Xiang, Y., Moss, B., 2017. Enigmatic origin of the poxvirus membrane from the endoplasmic reticulum shown by 3D imaging of vaccinia virus assembly mutants. Proc. Natl. Acad. Sci. U.S.A. 114, E11001–E11009.

Wu, X., Meng, X., Yan, B., Rose, L., Deng, J., Xiang, Y., 2012. Vaccinia virus virion membrane biogenesis protein A11 associates with viral membranes in a manner that requires the expression of another membrane biogenesis protein. A6. J. Virol. 86, 11276–11286.